Electronic structure of chemisorbed chalcogen atoms on Ni (*hkl*) surfaces

Pei-Lin Cao
Physics Department, Zhejiang University, Hangzhou, Zhejiang, People's Republic of China and Materials Research Center, Northwestern University, Evanston, Illinois 60201

D. E. Ellis and A. J. Freeman
Physics Department and Materials Research Center, Northwestern University, Evanston, Illinois 60201
(Received 6 August 1981)

Spectroscopic and bonding properties of sulfur, selenium, and tellurium atoms chemisorbed on different crystallographic faces of Ni are studied using self-consistent local-density molecular-cluster models. Adsorbate-substrate interactions lead to significant modification of the Ni $3d,4s,4p$ conduction bands in addition to forming the σ,π adatom levels located at ~ 5 eV below the Fermi energy. Adatom-adatom interactions are treated by S_2Ni_9 coupled clusters. Adatom bonding to the substrate is seen to be dominated by near-neighbor interactions through *sp* hybridization of the low-lying chalcogen *ns* level, and by π-bonding interaction of the *np* level. The (110) surface appears to have more ionic character than either (001) or (111). The calculated variation of adsorbate levels with adatom height above the metal surface supports low-energy-electron diffraction structural analyses. Partial densities of states derived from cluster orbital atomic populations are used to discuss features of photoelectron and Auger spectra.

I. INTRODUCTION

Numerous experimental studies have been performed in the last decade on the chemisorption of chalcogens on the Ni surface, including low-energy-electron diffraction (LEED),[1–9] photoelectron spectroscopy,[10–18] ion neutralization spectroscopy (INS),[19–22] ion scattering (IS), high-resolution electron-energy-loss spectroscopy (EELS), and Auger electron spectroscopy (AES).[23–26] These experimental studies have provided a wealth of information about the nature of chemisorption and the adsorbate-substrate interaction.

As a result of the LEED investigations, the geometrical structure of the chalcogens chemisorbed on the Ni surface appears to be well established: On the Ni(001) surface, the S atoms are located in the fourfold hollow sites about 1.3 Å above the first layer of Ni atoms (relative to the atom-center plane) for both the one-half monolayer $c(2\times2)$ (Ref. 27) and one-fourth monolayer $p(2\times2)$ cases. The Se and Te atoms are located in the same position but the vertical spacing is about 1.45 and 1.90 Å for the $c(2\times2)$ configuration and about 1.55 and 1.80 Å for the $p(2\times2)$.[1,2,4,8] On Ni(110), the S atoms are located in the fourfold hollow position for the $p(2\times2)$ coverage and the spacing is about 0.93 Å.[1,5] On Ni(111), the S atoms are located in the threefold hollow position for the $p(2\times2)$ structure and the spacing is about 1.40 Å.[1,5]

Ten years ago, Hagstrum and Becker[19] performed the first INS experiment on clean Ni(001) and on the same surface with $p(2\times2)$ and $c(2\times2)$ structures of O, S, and Se. The absorption of sulfur produces some extra structures in the spectra, the most prominent of which is situated about 4.5 eV below the Fermi level (E_F). In addition to the single-peaked feature of the ~ 2-eV wide Ni *d* band seen for clean Ni, the so-called double-peaked character of the adsorbate covered surface appears. The later ultraviolet photoelectron spectroscopy (UPS) experiments confirmed this double-peaked structure[12,13,16] and found additional structures not observed in INS including, for example, a peak at around -1.8 eV below E_F.[13] The other chalcogens show almost the same features in the spectra. These two chalcogen adsorbrate-induced levels were interpreted by Fisher[12] and Hagstrum and Becker[19] as arising from largely nonbonding (at -1.8 eV) and bonding (-4.5 eV) chalcogen *p* electrons. A relatively similar S induced structure has also been observed on the Ni (110) and (111) surfaces,[13] but S adsorption on these two surfaces is perhaps more complex than on the (001) surface because of the reconstruction[9] which takes place.

Both band-structure and molecular-cluster approaches have been utilized in analysis of the electronic structure of atom chemisorption on a Ni surface. The early work of Kasowski, using the non-self-consistent-layer—Korringa-Kohn-Rostoker (KKR) method, already gave essential qualitative features of the dispersion of sulfur *s* levels correctly.[28,29] Steady development of thin-film and slab-band techniques have now provided *self-consistent* methods capable of resolving details seen in excitation spectra, e.g., of O:Ni(001).[30]

Molecular-cluster approaches provide a computationally simpler scheme to treat localized interactions of chemisorbed species. Long-range interactions are either ignored, or treated approximately by embedding procedures. The cluster models have been very widely applied, using both semiempirical and more or less rigorous underlying electronic theories. In the context of *local density theory* (LD) used in most band-structure calculations, we may also mention previous cluster studies of X:Ni(001) where *X* is a first-row atom, and CO.[31,32] The self-consistent one-electron local density theory can thus be applied either in the context of bands or clusters, with sufficient predictive power to be a useful tool in surface analysis. This method is applied in the present work.

There are doubtless properties of chemisorbed molecules which require a precise *ab initio* treatment of electronic correlations, which are averaged in the LD theory. Walch and Goddard have applied the generalized valence-bond (GVB) technique to finite clusters such as NiS and Ni_4S, with the goal of directly determining geometry of the chemisorbed species.[33] The comparison of LD and GVB predictions of atomic binding energies and surface molecule geometries will provide a very significant measure of the role of explicit electron correlations in surface chemistry.

The aim of the present work is to develop a deeper insight into the bonding mechanism of chalcogen chemisorption on nickel, at the one-electron level. In particular, we wish to understand how different crystallographic Ni surfaces influence the character of chalcogen bonding orbitals and the accompanying modifications to the metal density of states (DOS) near E_F. The interaction between chalcogen atoms, which ultimately leads to bands several eV wide in the $c(2\times2)$ configuration, is studied by considering S_2Ni_9 clusters. The dichalcogen results are used to verify the correctness of the smaller cluster predictions, and to give an indication of the modification of S-Ni interactions with increasing coverage. Partial DOS have been successfully used to interpret the *LVV* Auger spectra of Bader and Richter[26] for S:Ni(001) and S:Ni(110); their results are briefly discussed.

II. THEORETICAL MODEL

A. Bonding geometries and local symmetry

The geometrical arrangement of the clusters for which we carried out electronic structure calculations is shown schematically in Fig. 1. For the

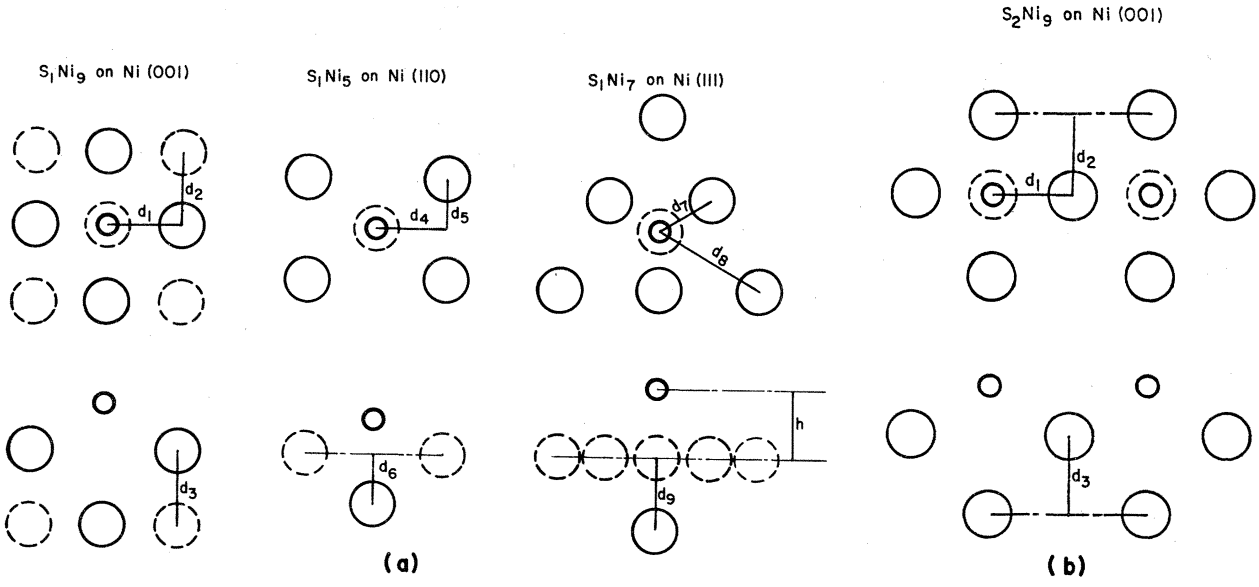

FIG. 1. Geometrical arrangement of the SNi_n clusters.

Ni(001) surface, the cluster consists of chalcogen atom in a fourfold "pocket" coordination site and five or nine Ni atoms; the fifth to ninth Ni atoms lie in the second metal plane. The C_{4v} symmetry used for both these $X\mathrm{Ni}_5$ and $X\mathrm{Ni}_9$ clusters, has four singly degenerate representation (a_1, a_2, b_1, b_2) and one doubly degenerate representation (e). The larger S_2Ni_9 cluster has C_{2v} symmetry. For the Ni(110) calculations, the cluster consists of a S atom and five Ni atoms. The S atom is located at the fourfold pocket position,[33] and C_{2v} symmetry is also used here. The C_{2v} group has four one-dimensional irreducible representations: (a_1, a_2, b_1, b_2). For Ni(111), the SNi_7 model cluster is used, the seventh Ni atom lying in the subsurface plane. The S atom is in the threefold pocket site and C_{3v} symmetry is satisfied. The C_{3v} group has two singly degenerate representations (a_1, a_2) and one doubly degenerate representation (e). Symmetry allowing mixing of adatom orbitals into the several-point group representations is indicated in Table I. Values of the distance between atoms for the arrangements shown in Fig. 1 and given in Table II and represent bulk nickel spacing. Note that these clusters are too small, except for S_2Ni_9, to represent the $c(2\times2)$ coverage; instead they are good representations of the $p(2\times2)$ coverage. In the calculations, the vertical spacing, h, between chalcogen atom and the first layer of Ni atoms, is varied to determine structural sensitivity of the spectra.

B. Computational Method

The one-electron Hamiltonian in the local density $X\alpha$ model has been used in these studies. In Hartree atomic units, it is given by

$$H(\vec{r})=-\tfrac{1}{2}\nabla^2+V_C(\vec{r})+V_x(\vec{r}) , \tag{1}$$

where V_C is the Coulomb potential

$$V_C(\vec{r})=\sum_j \frac{-Z_j}{|\vec{r}-\vec{R}_j|}+\int \frac{d^3\vec{r}'\rho(\vec{r}')}{|\vec{r}-\vec{r}'|} \tag{2}$$

and V_x is a statistical exchange potential of the form[34]

$$V_x(\vec{r})=-3\alpha\left[\frac{3}{8\pi}\rho(\vec{r})\right]^{1/3} \tag{3}$$

In (2) and (3), $\rho(\vec{r})$ is the electron density at position $\vec{r}$ and α is an exchange-correlation scaling parameter which is normally chosen as $\frac{2}{3}\le\alpha\le1$. Here it is chosen to be 0.7 for all calculations.[35]

The molecular wave functions are approximated by a linear combination of symmetry orbitals $\phi_i(\vec{r})$ as

$$\psi_n(\vec{r})=\sum_i \varphi_i(\vec{r})C_{in} , \tag{5}$$

where the symmetry orbitals are taken to be linear combinations of atom-centered functions. Solving the secular matrix equation

$$HC=ESC \tag{5}$$

determines the coefficients C_{in} where H and S represent the Hamiltonian and the overlap matrices, respectively.

The discrete variational method (DVM) is used to calculate the H and S matrices by a numerical integration procedure with a weighted sum over a set of (relatively few) sample points.[36,27] Thus, for example, we find that the largest difference in the energy levels calculated with 1200 points and 3600 points is about 0.18 eV for level $5a_1$ of the SNi_5 cluster. In the calculations reported here, about 2000 points were used for the SNi_5, SNi_9, $S_2Ni_9(001)$, $\mathrm{SNi}_5(110)$, and the $\mathrm{SNi}_7(111)$ clusters.

TABLE I. Symmetry allowed mixing of adatom orbitals into various point group representations.

Group	C_{4V}	C_{2V}	C_{3V}
Orbital character			
s	a_1	a_1	a_1
p_z	a_1	a_1	a_1
p_x,p_y	e	b_1,b_2	e
d_{z^2}	a_1	a_1	a_1
d_{xz},d_{yz}	e	b_1,b_2	e
d_{xy}	b_2	a_2	e
$d_{x^2-y^2}$	b_1	a_1	e

TABLE II. Values of the distances between atoms (in Bohr units) for the arrangement shown in Fig. 1.

d_1	d_2	d_3
3.3293	3.3293	3.3293
d_4	d_5	d_6
3.3293	2.3542	2.3542
d_7	d_8	d_9
2.7184	5.4367	3.8443

The molecular wave functions and eigenvalues were determined using the self-consistent charge (SCC) approximation to the potential.[38,39] From Mulliken gross orbital populations[40] for the symmetrized basis functions, the cluster charge density was decomposed approximately as

$$\rho_{\text{cluster}}=\sum_i f_i \mid \psi_i(\vec{r}) \mid^2 \simeq \sum_{\nu nl} f_{nl}^{\nu} \mid R_{nl}(r_\nu) \mid^2 = \rho_{\text{SCC}} , \quad (6)$$

where f_i is the occupation number for the ith eigenveotor which is determined by Fermi-Dirac statistics and f_{nl}^{ν} is the population for atom ν of the nl atomic orbital. Self-consistency is obtained when the input and output atomic-orbital populations are equal.

The basis functions were obtained from numerical solutions of the free-atom problem. In the present procedure, the S $1s,2s,2p$ and the Ni $1s$-$3p$ core orbitals have not been varied; that is, we have used a "frozen-core" approximation. For the valence electrons, the S $3s,3p,3d$ (Se $4s,4p,4d$, Te $5s,5p,5d$) and Ni $3d,4s,4p$ orbitals are included in the variational procedure.

In order to compare the theoretical results with the photoemission spectra and INS orbital energy spectra, the local density of states (LDOS), and total DOS are evaluated. The LDOS is represented by

$$d_{nl}^{\nu}(E)=\sum_p f_{nl,p}^{\nu} \frac{\sigma/\pi}{(E-\epsilon_p)^2+\sigma^2} , \quad (7)$$

where $f_{nl,p}^{\nu}$ is the population contribution from atom ν state nl to the p'th molecular orbital. The Lorentzian width parameter σ was chosen to be 1 eV,[35] in order to smooth out the discrete level structure into bands. By summing over all the local DOS, we can get the total DOS

$$D(E)=\sum_{\nu nl} D_{nl}^{\nu}=\sum_p \frac{\sigma/\pi}{(E-\epsilon_p)^2+\sigma^2} . \quad (8)$$

In order to discuss the Auger spectra, we adopt the simplest possible model of the two-electron process, writing the energy conservation requirement as

$$E_c=E_i+E_j-T .$$

Here E_c is the energy of the core level c, E_i is the energy of the valence level "i" from which a one-electron jumps to fill the core hole, E_j is the energy of the second valence level, and T is the observed kinetic energy of the emitted valence electron. If all relaxation and correlation effects are ignored, a convolution of the ground-state LDOS can be used to give a rough interpretation of the Auger spectra. The contribution of a given (i,j) valence pair to the AES signal can then be written (assuming constant transition probability matrix elements)

$$D_{ij}(T)=\int_{-\infty}^{E_F} D_i(\epsilon)D_j(E_c+T-\epsilon)d\epsilon . \quad (9)$$

While it is clear that core-hole binding-energy shifts (screening effects), and correlations among the several unfilled shells will produce significant shifts and splittings in the AES,[41–44] it is interesting to see what are predictions of the ground-state-level distributions.

III. RESULTS

A. Ground-state levels and bonding character

The theoretical ground-state valence levels for the different S_nNi_m clusters on the 3 different Ni surface are shown in Fig. 2. From Fig. 2 we can see that the main features of the level scheme for all configurations are rather similar, in agreement with the relative similarities of S induced structure observed on Ni(001), (110), and (111) in INS and UPS mentioned above. In all these cases, the lowest energy level shown is $1a_1$ consisting mainly of the S $3s$ level and mixed with the nearest neighbor Ni $4s$, $4p$, and $3d$ levels. It is well known that the bonding character of a molecular level can be determined by evaluating its derivative $\partial\epsilon_i/\partial h$; a positive derivative corresponds to a bonding orbital while a negative value indicates that it has antibonding character.[45] From this point of view all of these $1a_1$ levels have strong bonding character, with $\partial\epsilon/\partial h \simeq 2.3$ eV/bohr. From the geometry of the three different surfaces, it is clear that the shorter the distance between the S atom and the nearest Ni atom, the deeper the energy of the $1a_1$ level.

Above the bonding "S $3s$" level we find structure arising from interaction of S $3p$ levels with the substrate. In the SNi_5(001) cluster, the $1e$ and $3a_1$ levels, representing the (p_x,p_y) and p_z orbitals, respectively, are seen to be split and shifted in energy in quite different ways by interaction with Ni atoms. This picture of strongly bonded $p\pi$ levels, with the weaker $p\sigma$ interaction dominated by the subsurface (second plane) Ni atom, is quite similar to that found for O:Ni(001).[31] The addition of further

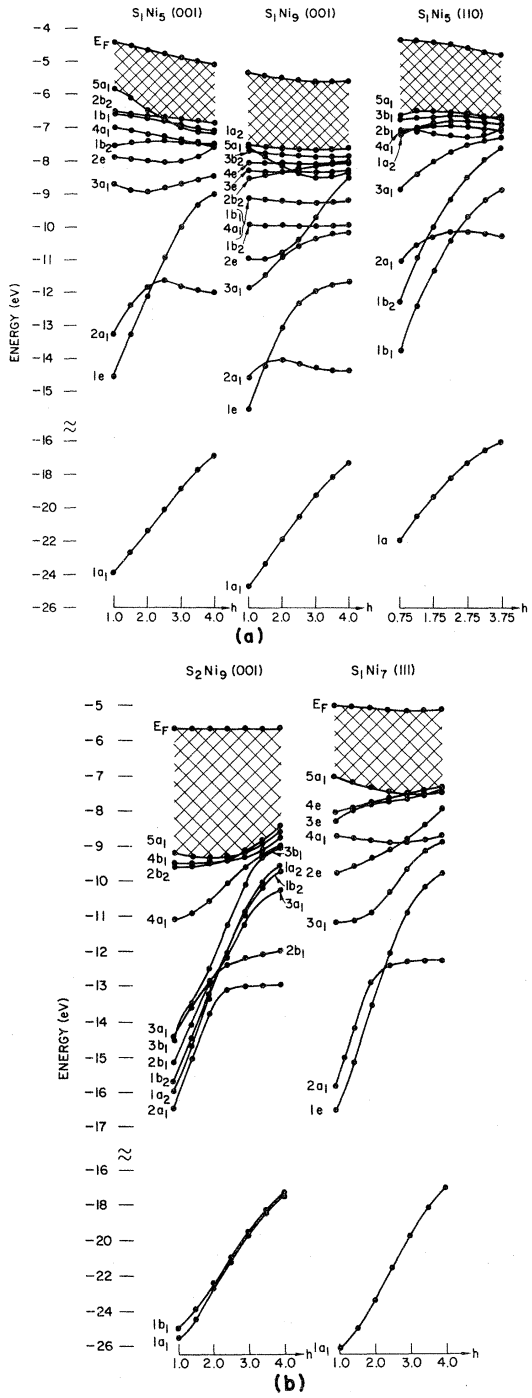

FIG. 2. The ground-state valence levels and their variation with height h for the different S_nNi_m clusters on the 3 different Ni surfaces.

second plane atoms (SNi_9) does not significantly modify this result, so that the bonding really can be considered to be a local phenomenon. Similarly, addition of adatom-adatom interactions (S_2Ni_9) introduces level doublings, e.g., $2a_1 \rightarrow 2a_1, 2b_1$, without altering the essential picture. The two additional surface orientations considered, (111) and (110), further verify the relatively stronger nature of $p\pi$-substrate interaction at reasonable heights above the metal surface. The bonding character of these orbitals and the energy levels of the S_2Ni_9 cluster will be discussed in detail below.

A Mulliken population analysis of the results for the different clusters has been used to determine their bonding character in a more quantitative sense. The variation with h spacing of the gross atomic charges Q_S for the S atom and $Q_{\rm I}, Q_{\rm II}$ for the nearest and the second nearest Ni atoms for these clusters are shown in Table III. A transfer of charge to the chalcogen atom is expected as it approaches the metal surface. As can be seen from the Table, the charge transfer is monotonic with h for Ni(001) and (110) configurations. At the equilibrium positions (as determined by LEED analyses) the Q_S values are -0.49 and -0.57 electrons for (001) and (110) cases. These values are thus found to be quite a bit smaller than the formal 2^- valency of sulfur would suggest, in accordance with results of many other studies on ionic compounds. The addition of further interactions with substrate (SNi_9) and between adatoms (S_2Ni_9) change the Q_S value for (001) geometry to -0.44 and $-0.47e^-$, respectively, again indicating the rather local nature of the S-Ni bonding interaction.

The sulfur charge Q_S for the (111) configuration is seen to pass through a maximum for $h \simeq 2.2$ a.u., with a value of $-0.45e^-$. Referring to Fig. 1, we see that the Ni-S distance, for a given height h, is less for (111) than for either (001) or (110) faces. The maximum charge transfer, as measured by the Mulliken populations, occurs for $R(\text{Ni-S}) \simeq 3.5$ a.u. for (111), somewhat shorter than the estimated equilibrium. The equilibrium value $-0.45e^-$ for Q_S is rather close to that for the (001) face; the (110) face is seen to form a slightly more ionic bond.

For a more detailed understanding of the bonding, we describe the individual atomic-orbital contributions. The variation of the occupation numbers of the S $3s, 3p, 3d$ orbitals with h are shown in Fig. 3. When h decreases and the S—Ni bond is forming, the S $3s$ population *decreases* and the S $3p$ population increases monotonically. Hence the interaction between the substrate Ni and the adsorbed S atom not only causes the transfer of charge from Ni to S, but also leads to the excitation of $3s$ electrons (hybridization) to $3p$ in S. The

TABLE III. The gross atomic charges (Q_S for the S atom, Q_I and Q_{II} for the nearest and the second-nearest Ni atoms), the Fermi energies (in eV) and their variation with height h (in Bohr) for several surface clusters.

			SNi_5 on Ni(001)				
h	1.0	1.5	2.0	2.5[a]	3.0	3.5	4.0
Q_S	−0.62	−0.60	−0.55	−0.49	−0.45	−0.42	−0.40
Q_I	0.18	0.19	0.18	0.15	0.14	0.12	0.10
Q_{II}	−0.11	−0.15	−0.15	−0.12	−0.09	−0.05	−0.02
E_F	−4.42	−4.52	−4.64	−4.76	−4.88	−4.99	−5.06
			SNi_5 on Ni(110)				
h	0.75	1.25	1.75[a]	2.25	2.75	3.25	3.75
Q_S	−0.64	−0.61	−0.57	−0.52	−0.49	−0.47	−0.44
Q_I	0.20	0.21	0.22	0.22	0.22	0.22	0.21
Q_{II}	−0.15	−0.24	−0.31	−0.36	−0.39	−0.41	−0.41
E_F	−4.37	−4.40	−4.46	−4.51	−4.60	−4.68	−4.73
			SNi_7 on Ni(111)				
h	1.0	1.5	2.0	2.5[a]	3.0	3.5	4.0
Q_S	−0.41	−0.43	−0.45	−0.45	−0.42	−0.39	−0.36
Q_I	−0.22	−0.20	−0.17	−0.17	−0.20	−0.23	−0.24
Q_{II}	0.31	0.30	0.30	0.30	0.31	0.32	0.33
E_F	−5.01	−5.04	−5.10	−5.16	−5.18	−5.16	−5.15

	XNi_9 on Ni(001) at equilibrium position		
	SNi_9	$SeNi_9$	$TeNi_9$
h	2.5	2.7	3.5
Q_X	−0.443	−0.356	−0.166
E_F	−5.55	−5.65	−5.61

[a] Approximate equilibrium position.

population of $3d$ orbitals for Ni atoms remains almost constant, about 8.5, for all these clusters and for all h values. This fact indicates that the $3d$ orbitals of Ni play an indirect role in the chemisorption of S atoms on a Ni surface. This result is similar to that for the chemisorption of CO on Ni.[32,45]

Now we discuss the ground-state levels in more detail for SNi_5 on Ni(001). From the C_{in} eigenvectors [cf. Eq. (4)], we not only know that the $1a_1$ level is fundamentally derived from the sulfur $3s$, but also that the $2a_1$ level is a strongly mixed orbital between sulfur $3s$, $3p$, $3d$, and the appropriate symmetric Ni state. When $h \to \infty$, this level approaches an a_1 state of the isolated metal cluster, essentially forming the bottom of the conduction band. The doubly degenerate energy level, $1e$, is principally derived from the sulfur $3p_x$ and $3p_y$ orbitals mixing with the $Ni_I 4s$ orbital. The orbital $3a_1$ is derived from sulfur $3p_z$ mixing mainly with Ni_I (Ni atoms on surface) $3d$ states. The π-bonding $1e$ state has the strongest bonding character, with $\partial\epsilon/\partial h \simeq 2.5$ eV/bohr. When h is larger than about 2.5 a.u. the $2a_1$ level has nonbonding character, but when $h < 2$ a.u., it acquires bonding character by mixing of S $3s$ with $3p$ Ni_{II} orbitals. The $3a_1$ level has a weak bonding character for $h \geq 2.0$ a.u. Among other features the $2e$ level contains noticeable contributions from sulfur $3d_{xz}$ and $3d_{yz}$ orbitals. The S $3d$ character of occupied states amounts to $0.1-0.2e^-$, as shown in Fig. 3. Higher lying levels belong essentially to the Ni d bands, so their energy eigenvalue change is rather small with h.

In order to examine cluster size effects and adatom-adatom interactions, we show in Fig. 4 valence levels of SNi_5, SNi_9, and $S_2Ni_9(001)$, at the equilibrium height $h = 2.5$ a.u. The cluster levels are aligned to a common Fermi energy to reveal significant shifts and splittings. First, let us see the effects of adding subsurface Ni_{II} atoms; i.e., $Ni_5 \to Ni_9$. The $1a_1$ "S $3s$" level is destabilized by 0.4 eV while the $1e$ "S $3p\pi$" is stablized by 0.6 eV. These shifts are an indirect effect of Ni—Ni bonding since the direct overlap with the added subsurface atoms is small. The bottom of the conduction

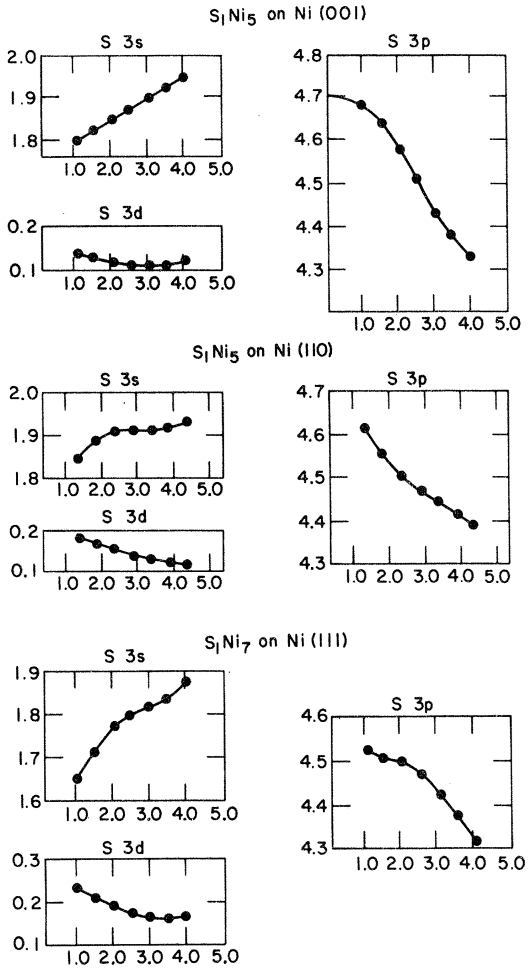

FIG. 3. Orbital population for the sulfur $3s, 3p, 3d$ orbitals and their variation with h.

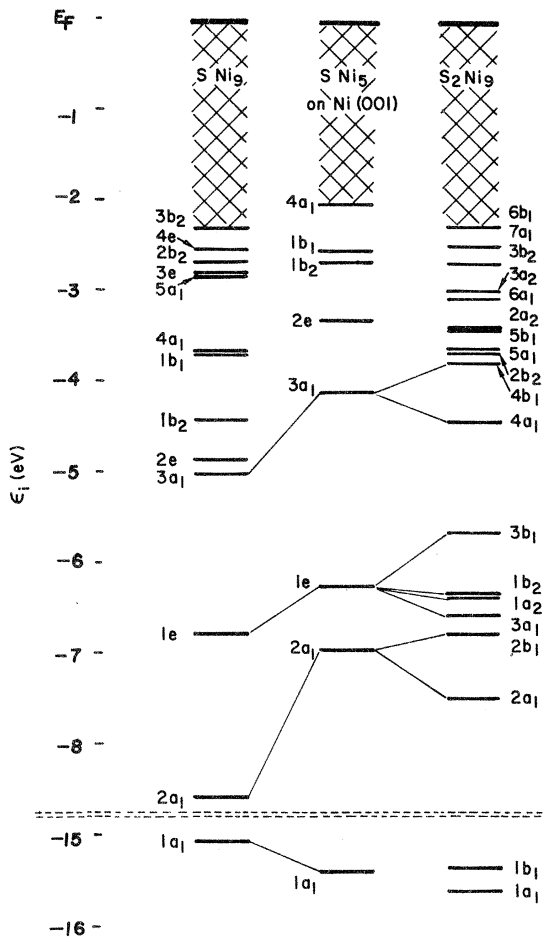

FIG. 4. The ground-state energy levels at $h = 2.5$ a.u. for the SNi_5, SNi_9, and S_2Ni_9 clusters.

band, $2a_1$, is lowered by 1.5 eV, yielding an improved estimate of the Ni band width of ~ 8.5 eV. This can be compared to the total band width of ~ 9 eV found in band-structure calculations on bulk nickel.

Turning now the S-S interaction, we consider the S_2Ni_9 cluster. Owing to the direct overlap between states of the two S atoms, and due to direct interaction via the substrate, the S-dominated levels are shifted and split. With the cluster symmetry reduced from C_{4v} to C_{2v}, we find $1a_1 \rightarrow (1a_1, 1b_1)$, $2a_1 \rightarrow (2a_1, 2b_1)$, and $1e \rightarrow (3a_1, 1a_2, 1b_2, 3b_1)$ with the bonding symmetric a_1 orbitals lying lower than the antibonding b_1 antisymmetric states. The similar splitting of the $3a_1$ level again indicates strong admixtures of S $3p_z$ character. The "S $3s$" band has an estimated width of ~ 0.25 eV. The S $3p_z$ contributions add to the bottom of the π band, and to the bottom of the Ni conduction band.

The different crystallographic faces can be characterized by the surface density of Ni atoms, which is 1.14, 1.61, and $1.85 \times 10^{15}/\text{cm}^2$ for (110), (001), and (111) surfaces, respectively. For chemisorption in the hollow position, it follows that the Ni-S distance $d(hkl)$ for a given height above the surfaces, is $d(111) < d(001) < d(110)$. At a height of 2.5 a.u. the corresponding bond lengths are 3.69, 4.16, and 4.78 a.u. In Table IV we display the influence of bond length on the $3s$ and $3p_\pi$-like

TABLE IV. The energy levels $1a_1$ and $1e_1$ on three different Ni surfaces.

	$E_i - E_F$	SNi_7 on Ni(111)	SNi_5 on Ni(001)	SNi_5 on Ni(110)
	$1a_1$	-16.01	-15.42	-13.23
$1e$ or	$1b_1$	-7.21	-6.23	-5.55
	$1b_2$			-4.20
	d (a.u.)	3.69	4.16	4.78

bonding chemisorption levels. It is evident that binding energy increases as bond length decreases, similar to the behavior with height on a particular crystallographic face. For the rather open (110) structure, the subsurface Ni_{II} atom plays an important role, the Ni_{II}-S distance being 4.85 a.u. in the above example.

From general bonding arguments one expects the equilibrium nearest-neighbor distance to be similar for the different (*hkl*) faces, with a systematic dependence on the number of coordinating Ni atoms. The LEED analyses suggest equilibrium heights of 2.64, 2.5, and 1.7 a.u. for the (111), (001), and (110) faces with the corresponding bond lengths of 4.16, 3.79, and 4.05 a.u. For the (110) face the single Ni_{II}-S bond is shorter than the fourfold Ni_I-S first layer bonds. For comparison, bond lengths in bulk compounds like NiS, NiS_2, and Ni_3S_2 range from 4.3—4.5 a.u., so the surface bonds are predicted to be appreciably shorter in every case.

The valence level structure for different equilibrium (*hkl*) geometries, referenced to a common Fermi energy, is shown in Fig. 5. We see that the binding energy of the chemisorption levels is directly related to the surface density: (111) > (110) > (110). We show in a later section that these features correlate well with photoelectron and AES data.

The correspondence between cluster models, LEED analysis of structure, and spectroscopic data can be further developed by comparing the isoelectronic S, Se, and Te series. The increasing ionic radius and decreasing electronegativity should lead to simple trends in the structural and spectrocopic parameters which can be checked by theory. Ground-state energy levels of SNi_9 $SeNi_9$, and $TeNi_9$ (001) clusters were calculated at the LEED equilibrium heights of 2.5, 2.7 and 3.5 a.u., respectively. The valence levels, shown in Fig. 6, are indeed very similar; the calculated Fermi energy of −5.6 eV differs by less then 0.1 eV from one cluster to another. The splittings between $np_\sigma(3a_1)$ and $np_\pi(1e)$ levels are 1.75, 1.69, and 1.64 eV for S, Se, and Te, respectively, and are thus nearly constant. The most obvious difference between the spectra is the destabilization of the Te 5*s* ($1a_1$) level; however, it is likely that relativistic effects not considered here will partially compensate this shift. The calculated adatom charges of −0.44, −0.36, and −0.17 for S, Se, and Te correlate well with the electronegativity values of 2.5, 2.4, and 2.1 eV, respectively[46]

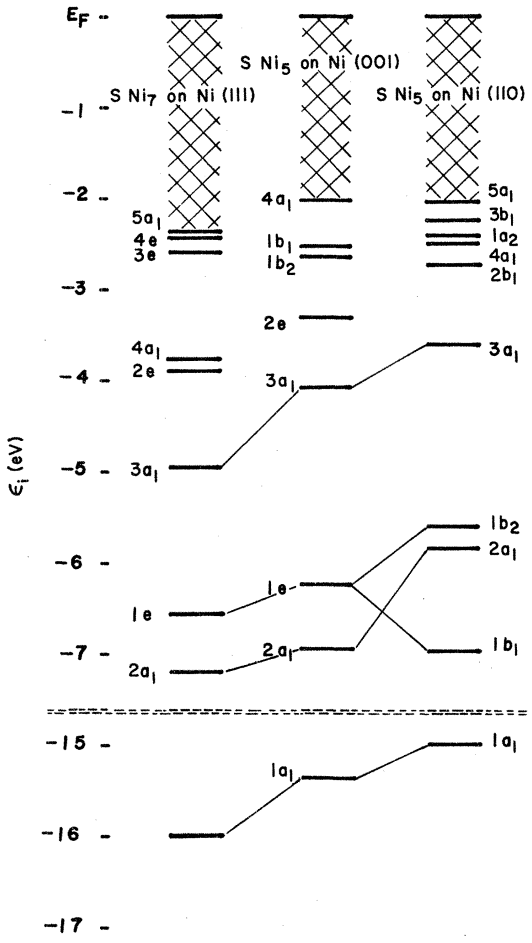

FIG. 5. The ground-state energy levels for SNi_5(001), SNi_5(110) and SNi_7(111) at the equilibrium position.

B. Excitation energies determined from self-consistent transition-state calculations

Before we discuss the theoretical DOS and compare it with x-ray photoelectron spectroscopy (XPS), UPS, and INS results, we first discuss the influence of final-state relaxation effects. Because of these relaxation effects, the local density ground-state MO eigenvalues for small molecules and atoms generally do not represent one-electron binding energies very well. Fortunately, Slater's transition-state procedure has been shown to be adequate for describing such effects with in the one-electron framework.[34,47,48] In the transition-state (TS) approach, one considers an excitation from an initial state i to a final state j in which the occupation number q_i is decreased by unity and q_j is increased by unity. A theorem is derived which

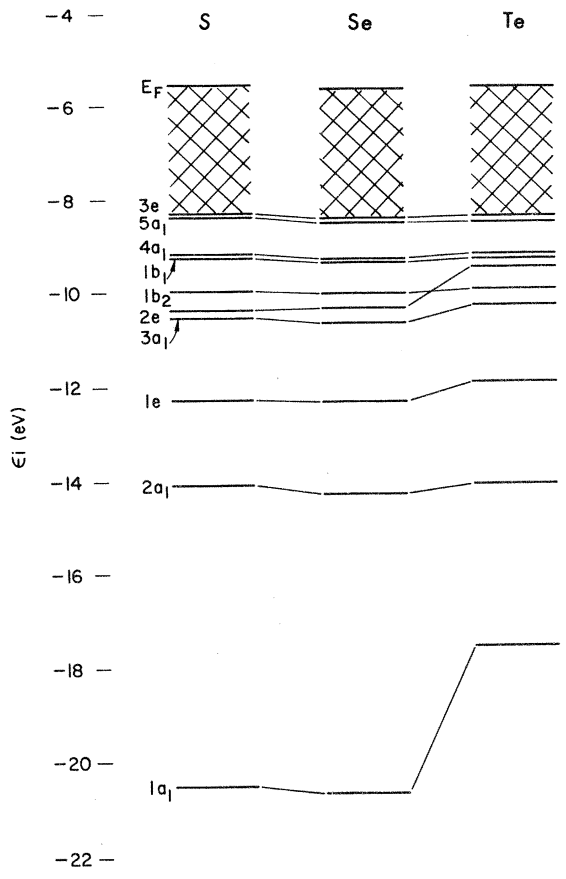

FIG. 6. The ground-state energy levels for SNi_9, $SeNi_9$, and $TeNi_9$ clusters at the equilibrium positions.

shows that to high accuracy, this excitation energy is given by the eigenvalue difference $\epsilon_i - \epsilon_j$ of a single self-consistent calculation for a state which has occupation numbers which are the average of those for the initial and final states (the so-called TS). For the TS, this result is quite close to the difference in total self-consistent energies of the system. For ionizing excitations in which the excited electron is removed to infinity, the ionization energy of level i is just the negative of the eigenvalue of this electron in a TS in which it is half-occupied (and half-removed).[34]

Transition-state calculations were made for several ionization levels of SNi_9 at $h=2.5$ and $SeNi_9$ at $h=2.7$. The results are given in Table V where ϵ_i are the ground-state eigenvalues and ϵ_i^{TS} are the eigenvalues obtained from the transition-state calculations (relative to E_F). It is clear from these results that the largest change is for the lowest energy $3s$ ($1a_1$) state (~ 0.9 eV); the change for the $2a_1$ state is only about 0.2 eV and for $3a_1$ only about 0.1 eV. Since we expect that the shifts from the upper levels will be even smaller due to metal donation of the screening charge, we neglect the final-state relaxation effects in the following discussion of the comparison of our calculated DOS with experiment.

C. Density of states and comparisons with experiment

The total and projected DOS for the clusters of the different surface orientations are given in Figs. 7–12. In each case, the area under the curve for $\epsilon < E_F$ is normalized to equal the occupation number in either the system (i.e., total number of electrons for the total DOS) or in the atomic orbital considered. Similar quantities are presented together in order to make visual comparisons easier.

In Fig. 7 are given the total DOS for S chemisorption on (001), (110), and (111) nickel clusters,

TABLE V. Ionization potentials obtained from ground-state and transition-state calculations, in eV. Relaxation shifts are indicated.

SNi_9 on Ni(001)	$1a_1$	$2a_1$	$3a_1$
$E_i - E_F$	−15.03	−8.56	−5.00
$E_i^{TS} - E_F^{TS}$	−15.92	−8.77	−5.13
$(E_i - E_F) - (E_i^{TS} - E_F^{TS})$	0.89	0.21	0.13
$SeNi_9$ on Ni(001)	$1a_1$	$2a_1$	$3a_1$
$E_i - E_F$	−15.03	−8.63	−5.00
$E_i^{TS} - E_F^{TS}$	−15.93	−8.84	−5.13
$(E_i - E_F) - (E_i^{TS} - E_F^{TS})$	0.90	0.21	0.13

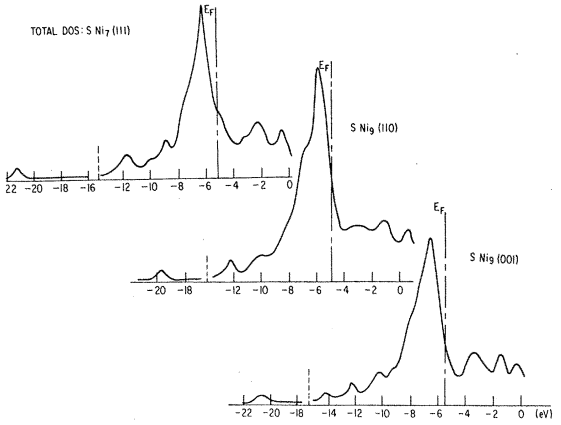

FIG. 7. The total density of states for SNi_x clusters on Ni (001), (110), and (111) crystal faces.

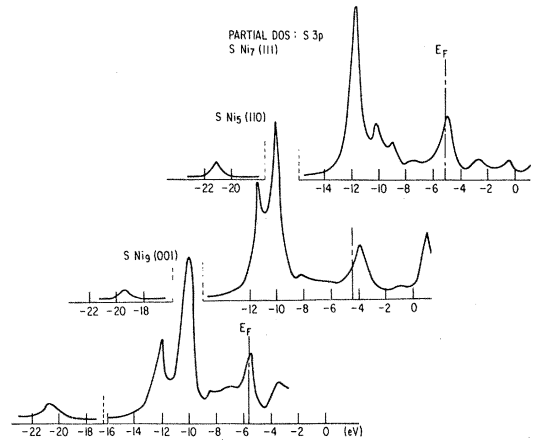

FIG. 9. The sulfur $3p$ partial DOS for Ni (001), (110), and (111) faces.

calculated at the equilibrium height (i.e., 2.50, 1.70, and 2.64, respectively). The main Ni d-band structure around E_F is seen to be similar in the three cases; however, there are differences in detail which will be discussed in connection with partial densities. Below the main d structure appear four additional peaks induced by the absorbed atom, consisting primarily of S bonding $3s,3p\pi,3p\sigma$ levels mixed to varying degrees with substrate $3d,4s,4p$ character. Although structures above the Fermi energy are clearly visible.

The lowest level $1a_1$ is dominated by S $3s$ character as shown in Fig. 8. This peak lies at ~ -20.6 eV for (001) and (111) faces, but is shifted to ~ 1 eV lower binding energy on the (110) face. We suggest that this difference is a measure of the more ionic nature of the (110) surface bond

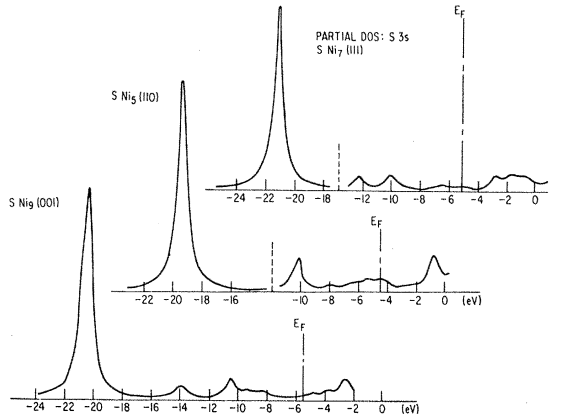

FIG. 8. The sulfur $3s$ partial DOS for Ni (001), (110), and (111) faces.

to sulfur. A small amount of S s character is visible throughout the higher chemisorption levels and conduction band as well.

The S $3p$ character is depicted in Fig. 9. For SNi_9(001) the peaks at -12.3 and -10.5 eV arise fundamentally from $3p_\pi(1e,2e)$ and the $3p_\sigma(3a_1)$ bonding states. The main $(2e,3a_1)$ peak thus falls 4.9 eV below the Fermi level, in good agreement with INS (Ref. 21) and UPS (Refs. 10, 12, and 18) ($\sim 4.5-5$ eV) measurements. For SNi_5(110) we find the $3p_\pi(b_1,b_2)$ peaks at $\sim 5.5-6.5$ eV below E_F. These results confirm the shift to higher binding energy on the (110) face found by UPS (Ref. 13) and INS (Refs. 10 and 12); our values are a little larger than the ~ 5.0 eV experimental values. The $3p_\sigma$ peak loses intensity and moves up to 3.6 eV; the addition of second layer atoms, to form the SNi_9(110) cluster hardly changes the $3p$ contributions. The SNi_7(111) sulfur $3p$ LDOS reveals an intense peak at -11.8 eV, arising from nearly degenerate $1e$ and $2a_1$ levels, with a secondary $p_\sigma(3a_1)$ peak at -10.1 eV. Rhodin and Capehart[15,17] performed angle-resolved photoemission (ARUPS) experiments on S:Ni(111), finding two peaks, at 4.2 and 5.5 eV below E_F (-10.1, -11.5 eV). The higher lying peak was assigned to the a_1 level, and the lower peak, to e. In addition, these authors postulated a third state, of a_1 symmetry, lying below -20 eV; this state corresponds to our $1a_1$ level at -21 eV. Thus we find rather good agreement between theory and experiment for the (111) geometry; see Table VI. The peak centered around 5.0 eV below E_F in a second UPS study[13] seems to correspond to our $1e$ ($3p_\pi$) level, while the ion neutralization transition density

TABLE VI. The comparison between experimental and theoretical energy levels for sulfur absorbed on Ni(111).

	a_1	e	a_1
Experimental (Ref. 17)	−10.0	−11.5	below −20
Theoretical	−10.1 ($3a_1$)	−11.8 ($1e$)	−21.2 ($1a_1$)

peak[22] at ~4.0 eV corresponds to $3a_1$ ($3p_\sigma$). We suppose that the difference in transition probabilities for the very different UPS and INS processes is reponsible for emphasizing one peak over the other.

Turning now to the metal emission features, we compare in Fig. 10 the Ni $3d$-LDOS for surface atoms, Ni_I, in the (001) and (111) geometries and for the subsurface Ni_{II}(001) atoms. First, note that Ni_I(001) forms a two peak $3d$ band, with maxima at ~1 and ~2 eV below E_F. ARUPS experiments[13] clearly resolve the second peak, at 1.8−2.0 eV below E_F. The subsurface layer is seen to contribute mainly to the second peak, although the total band widths are similar. The Ni $3d$-LDOS for the (111) has similar 1 and 2 eV peak positions; further structure at ~9 eV is visible. For the (110) configuration, (not shown in the figure) a pronounced shoulder also falls at 1.9 eV, so this feature appears to be quite general.

The total densities of states for S, Se, and Te on Ni(001) are presented in Fig. 11. The main features; low-lying chemisorption peaks, intense Ni d band, and antibonding structure above E_F are seen to be very similar, as indeed is the case experimentally. The equilibrium heights of 2.5, 2.7, and 3.5 a.u., respectively, were used in the calculations. By examining the chalcogen np LDOS in Fig. 12, we can detect significant changes. The intense, mostly np_σ, main peak falls at 4.9, 4.5, and 3.8 eV below the Fermi energy for S, Se, and Te, respectively. This trend with atomic number is in good agreement with the INS (Ref. 21) and UPS (Refs. 10, 12, and 13) results. The presence of a nonbonding np peak essentially pinned at E_F is seen to be a general feature, independent of adatom and crystal face (see Fig. 9).

D. Interpretation of *LVV* Auger spectra of sulfur

Bader and Richter have examined the *LVV* Auger spectra of sulfur on different crystallographic faces of nickel as a function of coverage.[26] Typical results for $p(2\times2)$S:Ni(001) or (110) at coverage $\theta\simeq0.25$ are shown in Fig. 13. These authors have shown that principal features of the AES can be explained using the *unrelaxed ground state* S partial DOS (see Fig. 14). In view of recent discussions in the literature concerning hole-hole Coulomb interactions,[41] this result indicates that chemisorbed sulfur levels fall in the "band re-

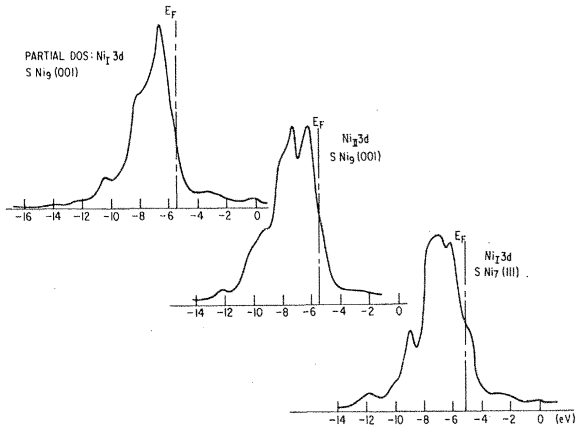

FIG. 10. The nickel $3d$ partial DOS for Ni (111) and (001) faces.

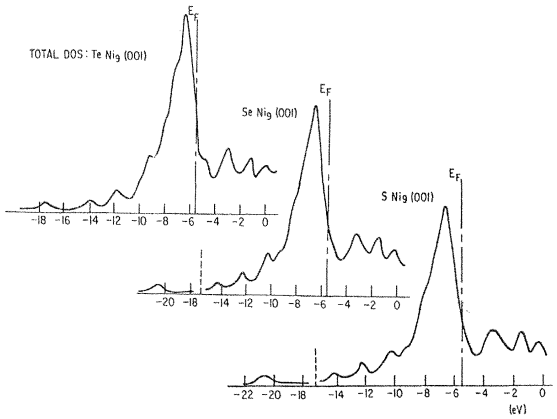

FIG. 11. The total DOS for S, Se, and Te on the Ni(001) face.

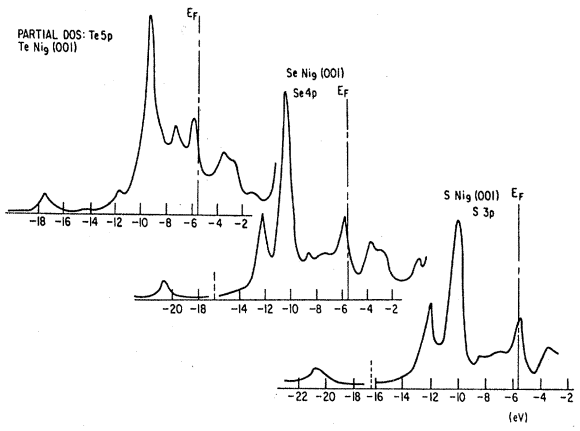

FIG. 12. The chalcogen *np* partial DOS on the Ni(001) face.

gime". That is, the two-hole states are so effectively screened by the metallic density that the effective Coulomb energy U must be rather small, <2 eV. The success in fitting relative intensities of the AES by separately weighting S 3*s* and 3*p* contributions lends support to semiempirical matrix-element schemes which have been applied to small molecules.[42,43]

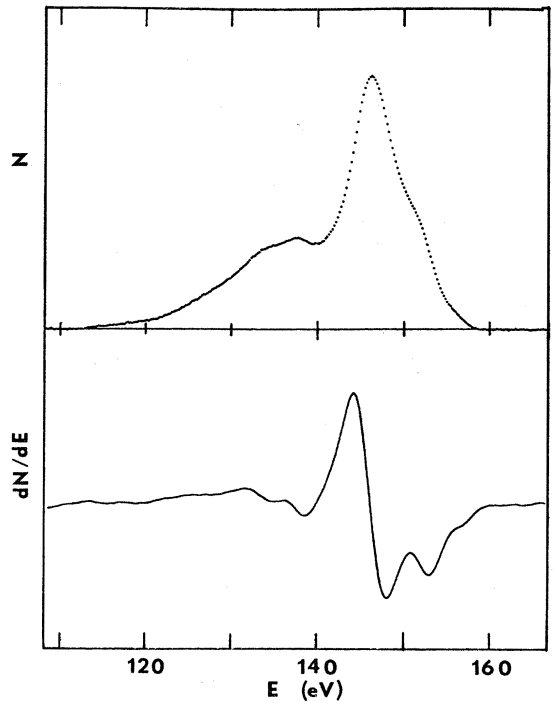

FIG. 13. Auger *LVV* spectra of Bader and Richter for $p(2\times2)$ S:Ni(110); counting rate $N(E)$ and derivative dN/dE versus kinetic energy. Smooth background substracted.

The weighted and broadened S 3*s*, 3*p* PDOS is shown as curve N' in Fig. 14. The "crystal field" splitting of $3p\pi$, $3p\sigma$ levels results in an asymmetrical main peak P_1. The remaining significant features are the nonbonding S 3*p* peak P_2 with maximum just above the Fermi energy and the S 3*s* peak "S". The convolution $N'\times N'$ doubles the energy range to ~40 eV, and display pairwise features of the parent spectrum. In order of increasing energy these features can be labeled P_2^2 (shoulder just below E_F), P_1P_2 (low-energy shoulder), P_1^2 (main peak), SP_2 and SP_1 (secondary peak ~21 eV) and S^2 (weak high-energy peak). The labeling thus indicates the particular two-electron hole state responsible for details of the experimental AES; the match is seen to be rather good. The comparison could probably be further improved by taking orbital relaxation into account, using the transition-state procedure. The S 3*s* level will exhi-

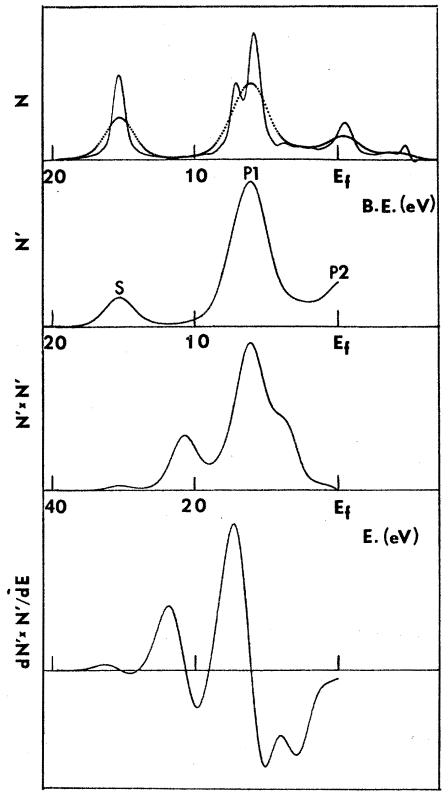

FIG. 14. Density of states analysis of Auger spectra. (a) S 3*s*, 3*p* LDOS for SNi_5(001) cluster-solid curve; and broadened with a Gaussian distribution of width 0.8 eV. (b) Broadened LDOS, reweighted as $N'=\frac{1}{3}N_s+N_p$ to simulate matrix element effects. (c) Self-convolution of N'. (d) Energy derivative of convolution function (from Ref. 26).

bit a differential shift to greater binding energy, moving "*S*" and "*SP*" features to lower kinetic energy in the Auger spectra.

IV. SUMMARY AND CONCLUSIONS

Energy levels, charge distributions, and densities of states were calculated for chalcogens chemisorbed on three different nickel surfaces. From comparison with photoelectron, ion neutralization, and Auger data we can conclude that the self-consistent Hartree-Fock-Slater molecular cluster model gives an adequate representation of one-electron features across the entire series of systems treated. Specific features seen in the *d*-band spectra; i.e., the two-peak structure at ~ 1.0 and ~ 2.0 eV below E_F are successfully reproduced, and interpreted using local densities of states. The LDOS results also reveal the considerable importance of chalcogen s-p_σ hybridization in forming the surface bond, in addition to the strong p_π-surface bonding interaction. The *np* LDOS also show three groups of peaks; the bonding chemisorption levels at ~ 5.0 eV below E_F, nonbonding structure pinned at E_F, and antibonding character located a few volts higher in energy. The antibonding level have not yet been described experimentally; they should become evident in electron-energy-loss spectroscopy, and in x-ray absorption near edge phenomena.

Comparison with the *LVV* Auger spectra of Bader and Richter[26] shows that the convolution of one-electron partial densities of states provides a useful interpretation of AES features. The substantial agreement between ground-state level predictions and experiment suggests that relaxation and hole-hole Coulomb interactions are effectively screened in chalcogen chemisorption. This can hardly be the case in general, so further comparison of theory with AES data for chemisorbed species would thus be very worthwhile.

ACKNOWLEDGMENTS

We thank S. D. Bader for helpful discussions and for permission to display his unpublished data. This work was supported by the NSF-MRL program through the Materials Research Center of Northwestern University (Grant No. DMR79-23573), and by the Office of Naval Research (Grant No. N00014-81-K-0438).

[1]P. M. Marcus, J. E. Demuth, and D. W. Jepsen, Surf. Sci. 53, 501 (1975).
[2]J. E. Demuth, D. W. Jepsen, and P. M. Marcus, Phys. Rev. Lett. 31, 540 (1973).
[3]C. B. Duke, N. O. Lipari, and G. E. Laramore, J. Vac. Sci. Technol. 12, 222 (1975).
[4]J. E. Demuth, D. W. Jepsen, and P. M. Marcus, Solid State Comm. 13, 1311 (1973).
[5]J. E. Demuth, D. W. Jepsen, and P. M. Marcus, Phys. Rev. Lett. 32, 1182 (1974).
[6]J. E. Demuth and T. N. Rhodin. Surf. Sci. 45, 249 (1975).
[7]D. W. Jepsen and P. M. Marcus, J. Phys. C 6, L307 (1973).
[8]M. Van Hove and S. Y. Tong, J. Vac. Sci. Technol. 12, 230 (1975).
[9]M. Perdereau and J. Oudar, Surf. Sci. 20, 80 (1970).
[10]H. D. Hagstrum and G. E. Becker, Proc. R. Soc. London Ser. A 331, 395 (1972); H. D. Hagstrum, Science 178, 275 (1972).
[11]K. Jacobi and C. V. Muschwitz, Solid State Commun. 26, 477 (1978).
[12]G. B. Fisher, Surf. Sci. 62, 31 (1977).
[13]T. T. Anh Nguyen and R. C. Cinti, Surf. Sci. 68, 566 (1977).
[14]S. P. Weeks and E. W. Plummer, Solid State Commun. 21, 695 (1977).
[15]T. W. Capehart and T. N. Rhodin, Surf. Sci. 82, 367 (1979).
[16]E. W. Plummer, B. Tanner, and N. Holzworth, Phys. Rev. B 21, 4306 (1980).
[17]T. N. Rhodin and T. W. Caprehart, Surf. Sci. 89, 337 (1979).
[18]K. Jacobi, M. Scheffler, K. Kambe and F. Forstman, Solid State Commun. 22, 17 (1977).
[19]H. D. Hagstrum and G. E. Becker, Phys. Rev. Lett. 221, 1054 (1969).
[20]G. E. Becker and H. D. Hagstrum, Surf. Sci. 30, 505 (1972).
[21]H. D. Hagstrum and G. E. Becker, J. Chem. Phys. 54, 1015 (1971).
[22]H. D. Hagstrum, J. Vac. Sci. Technol. 12, 7 (1975).
[23]H. H. Brongersma, J. Vac. Sci. Technol. 11, 231 (1974).
[24]S. Andersson, Surf. Sci. 79, 385 (1979).
[25]R. Rivan, Surf. Sci. 27, 267 (1971).
[26]S. D. Bader and L. Richter, Bull. Am. Phys. Soc. 26, 395 (1981) and unpublished data.

[27]Recent evidence suggests the existence of a second site for the related O:Ni(001) system, with reduced height 0.26 Å more characteristic of the bulk oxide: T. Upton and W. A. Goddard, Phys. Rev. Lett. 46, 1635 (1981); T. S. Rahman, J. E. Black, and D. L. Mills, *ibid.* 46, 1469 (1981).

[28]A. Liebsch, Phys. Rev. B 17, 1653 (1978).

[29]R. V. Kasowski, Phys. Rev. Lett. 33, 1147 (1974).

[30]C. S. Wang and A. J. Freeman, Phys. Rev. B 19, 4930 (1979).

[31]D. E. Ellis, H. Adachi and F. W. Averill, Surf. Sci. 58, 497 (1976).

[32]A. Rosen, E. J. Baerends and D. E. Ellis, Surf. Sci. 82, 139 (1979).

[33]S. P. Walch and W. A. Goddard, Surf. Sci. 75, 609 (1978). These authors argue in favor of a bridged configuration on the (110) surface, while we have chosen to model the pocket site assumed in LEED analyses.

[34]J. C. Slater, *The Self-consistent Field for Molecules and Solids* (McGraw-Hill, New York, 1974).

[35]E. J. Baerends, D. E. Ellis, and P. Ros, Chem. Phys. 2, 41 (1973); V. L. Moruzzi, A. R. Williams, and J. F. Janak, Phys. Rev. B 15, 2854 (1977); W. Kohn and L. J. Sham, Phys. Rev. 140, A1133 (1965).

[36]D. E. Ellis and G. S. Painter, Phys. Rev. B 2, 2887 (1970).

[37]T. Parameswaran and D. E. Ellis, J. Chem. Phys. 58, 2008 (1973).

[38]A. Rosén, D. E. Ellis, H. Adachi and F. W. Averill, J. Chem. Phys. 65, 3629 (1976).

[39]D. E. Ellis, G. A. Benesh, and E. Byrom, Phys. Rev. B 20, 1198 (1979).

[40]R. S. Mulliken, J. Chem. Phys. 23, 1833 (1955); 23, 1841 (1955).

[41]G. A. Sawatzky and A. Lenselink, Phys. Rev. B 21, 1790 (1980).

[42]B. I. Dunlap, P. A. Mills, and D. E. Ramaker, J. Chem. Phys. 75, 300 (1981).

[43]D. R. Jennison, Phys. Rev. B 18, 6996 (1978); 18, 6865 (1978).

[44]M. Cini, Solid State Commun. 24, 681 (1977); Phys. Rev. B 17, 2788 (1978).

[45]A. Rosén and P. Grundevik, Surf. Sci. 95, 477 (1980); L. S. Cederbaum, W. Domcke *et al.*, Z. Phys. B 21, 381 (1975).

[46]L. Pauling, *Nature of the Chemical Bond* (Cornell University Press, Ithaca, 1972).

[47]J. C. Slater and K. H. Johnson, Phys, Rev. B 5, 844 (1972); K. H. Johnson and F. C. Smith, *ibid.* 5, 831 (1972).

[48]E. J. Baerends, D. E. Ellis, and P. Ros, Chem. Phys. 2, 41 (1973); E. J. Baerends and P. Ros, *ibid.* 2, 52 (1973).